The organometallic active site of [Fe]hydrogenase: Models and entatic states

Marcetta Y. Darensbourg*, Erica J. Lyon, Xuan Zhao, and Irene P. Georgakaki

Texas A&M University, Department of Chemistry, College Station, TX 77843

The simple organometallic, $(\mu\text{-}S_2)Fe_2(CO)_6$, serves as a precursor to synthetic analogues of the chemically rudimentary iron-only hydrogenase enzyme active site. The fundamental properties of the $(\mu\text{-}SCH_2CH_2CH_2S)[Fe(CO)_3]_2$ compound, including structural mobility and regioselectivity in cyanide/carbon monoxide substitution reactions, relate to the enzyme active site in the form of transition-state structures along reaction paths rather than ground-state structures. Even in the absence of protein-based active-site organization, the ground-state structural model complexes are shown to serve as hydrogenase enzyme reaction models, H_2 uptake and H_2 production, with the input of photo- or electrochemical energy, respectively.

Since the discoveries of hydrogenases (H_2ases) in bacteria in 1931 (1, 2) and in Archaea in 1981 (3), their importance in all areas of natural sciences and their potential for technological application (for H_2 production as well as efficient H_2 uptake in fuel cells) (4, 5) have commanded extensive research effort. In fact, reports of the similarity in H_2 uptake and splitting by orga-nometallics such as $Co_2(CO)_8$ to produce $HCo(CO)_4$, a species that could easily reproduce the enzymes' activity assay of H/D isotope scrambling in H_2/D_2O mixtures (6, 7), appeared before the knowledge of metal content in the enzymes! The fact that a bimetallic was chosen as example demonstrated remarkable pre-science or, perhaps, just good luck (see below). The dicobaltoc-tacarbonyl analogy is attractive, particularly in view of the subse-quent determination of binuclear organometallic active sites in both Fe-only and [NiFe]H_2ases. Nevertheless, binuclear oxidative addition of H_2, with concomitant homolytic splitting and formal conversion to two hydrides as in the $H_2/Co_2(CO)_8$ reaction (8), is not accepted as the mechanism of H_2 activation in the metal-lohydrogenases. From pH-dependent studies it was shown that H_2 splitting and presumably H_2 formation occur in a heterolytic H^+/H^- manner (9–11). Subsequent removal of electrons from the metal hydride accounts for an energy-efficient use of H_2 as a cellular fuel: $H_2 \rightleftharpoons 2H^+ + 2e^-$. The reverse process produces H_2, which is the direction of reactivity to which most [Fe]H_2ases are committed (12, 13).

The heterolytic splitting of dihydrogen as a low-energy route to metal hydrides that are reactive toward reducible substrates has been known for decades (14, 15). The require-ments for the binding of H_2, producing stable (η^2–H_2)M com-plexes, are also well understood (16, 17). One of the assem-blies that nature has produced for such processes, perfected by evolution over billions of years and exacting exquisite con-trol over H_2 binding and release, is the subject of this article.

In our view, which is related to those expressed by Wächter-shäuser (18), Adams and Stiefel (19), as well as Fontecilla-Camps and coworkers (20), the ultimate ancestor of the distinctly organometallic active site of iron H_2ases is diiron-hexacarbonyldisulfide, i.e., a fragment of the mineral iron sul-fide, rendered molecular and mobilized by carbon monoxide (Fig. 1). Over the course of 4 billion years it has been developed by nature, perhaps initially as a template on which condensations of atoms and small molecules created rudimentary organic moi-eties, perhaps peptidic-like polymers. Later the catalyst became internalized within the protein, evolving to be protected from

the oxidizing environment of a maturing Earth. An entirely dif-ferent biosynthetic scheme would then be obligatory, resulting in a controlled synthesis of an extraordinary and sophisticated cata-lytic site. The existence and immobilization of diatomic ligands in the metallohydrogenases, both in [NiFe]H_2ase (21–23) and [Fe]H_2ase (24–29), is truly remarkable in current biochemistry in that carbon monoxide and cyanide are typically poisonous to all life forms.

Although such a catalytic role of CO-mobilized iron sulfide in chemical evolution as expressed above has not been sub-stantiated, it finds some support in experiments that have linked low valent primordial carbonylated iron–sulfur com-pounds to the synthesis of pyruvate in conditions that mim-icked hydrothermal vents and ancient environments (30). This concept readily suggests easy synthetic access to compounds that should model the active site of Fe-only H_2ase, which also begins with $(\mu\text{-}S_2)Fe_2(CO)_6$ (refs. 31 and 32; Fig. 1).

On an entirely different time scale, chemists have established the ability of the diirondisulfide of $(\mu\text{-}S_2)Fe_2(CO)_6$ unit to medi-ate organic transformations at sulfur (33, 34), including the syn-thesis of model complexes (35) of import to the discussion be-low. The parent model, $(\mu\text{-}pdt)Fe_2(CO)_6$ (pdt = $^-S(CH_2)_3S^-$), (35) is a complex that reproduces the Fe_2S_2 core fairly faithfully (36), including the three-light-atom S-to-S linker (Fig. 1). It re-acts with cyanide with complete regioselectivity in CN^-/CO ex-change, yielding one cyanide on each iron, $(\mu\text{-}pdt)[Fe(CO)_2(CN)]_2^{2-}$ (36–38). The coordination geometry of the dinuclear model complexes is that of a binuclear unit con-sisting of two edge-bridged square pyramids. The formal oxida-tion state of the iron is +1, and, to achieve an 18-electron count on each iron, a metal—metal bond is required, consistent with the observed Fe···Fe distance of 2.5 Å.

The [Fe]H_2ase active-site structure (39) defines what was known to be an unusual [6Fe6S] cluster, referred to as the H cluster or hydrogen-producing cluster. Protein crystallography resolved the H cluster into two components. A typical [4Fe4S] cluster is cysteine-bridged to an unusual [2Fe2S] unit. The former is one of several [4Fe4S] ferredoxin units positioned 12.5 Å apart that define the electron-transfer path from the buried active site to the exterior of the protein, a feature observed in structures of all metallohydrogenases. The [2Fe2S] unit is of sim-ilar composition and overall geometry as the organometallic model complexes with an Fe_2S_2 butterfly core and an Fe···Fe distance of 2.6 Å. They differ in the orientation of the two-edge-bridged square pyramids: The model complexes place "open" sites underneath the $\mu\text{-}S_2Fe_2$ unit; the binuclear active site has one square pyramid inverted with respect to the other. This gives the appearance of an open site on a single iron in one form of the enzyme, denoted by the dashed circle in Fig. 2. The appar-ent open site in the reduced form, H_{red} (25, 26), of the enzyme, presumed to be $Fe^I Fe^I$, might be occupied by a hydrogenic spe-cies, H_2 or H^-, undetected by protein crystallography. The site is
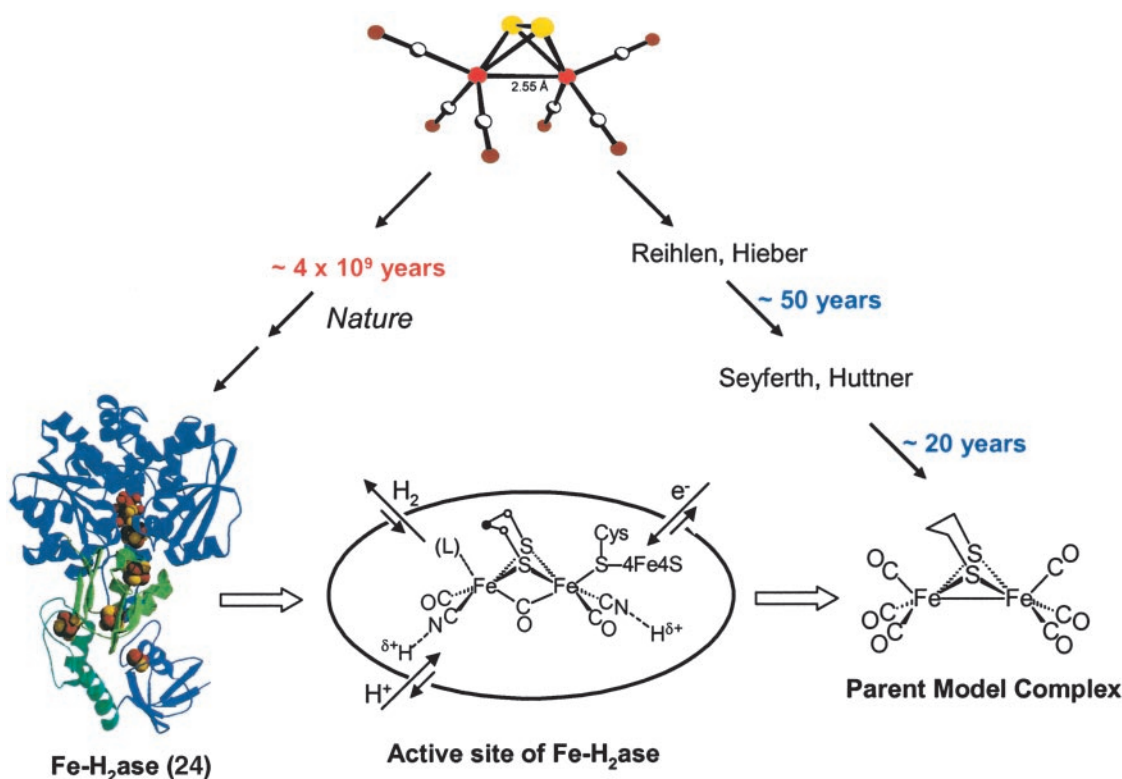
Fig. 1. Representation of the evolution of CO-mobilized iron sulfide in nature to yield the active site of [Fe]H₂ase and in chemists' laboratories to yield model complexes. [The structure of [Fe]H₂ase is reprinted with permission from Peters *et al.* (24) (Copyright 1998 American Association for the Advancement of Science).]

definitely occupied by H_2O in the oxidized form, H_{ox} (24), and by CO in the CO-inhibited, oxidized form of the enzyme (27). The latter, established by both crystallography and IR spectroscopy (40, 41), is a strong indicator of substrate site binding.

The identity of the three light atoms that link sulfurs in the enzyme active site cannot be unambiguously determined by protein crystallography. If, as initially modeled (25), all three are carbon, propane dithiolate would be an entirely new organic cofactor in biochemistry. A supposition that the central atom might be a heteroatom such as nitrogen (26), introducing an internal base proximal to the H_2-binding or H_2-producing site and well positioned to either deliver or extract protons, is attractive (42). However, it is not, at the time of this writing, verifiable; the biosynthesis of [Fe]H₂ase remains unknown. A synthetic route to $(\mu\text{-SCH}_2\text{N(Me)CH}_2\text{S})[\text{Fe(CO)}_3]_2$ derived from condensation of methyl amine and formaldehyde (Eq. **1**) lends support to the supposition that iron sulfide might template small-molecule transformation to an elaborated organic moiety (43).

$$NH_2Me + HCHH + (\mu\text{-SH})_2[\text{Fe(CO)}_3]_2 \longrightarrow \quad [1]$$
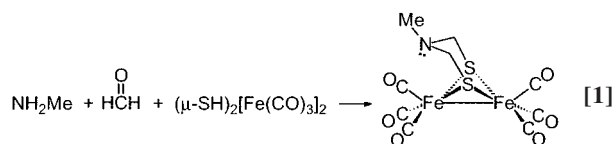
The inverted square pyramid that exists in the Fe_2S_2 unit on the iron distal to the [4Fe4S] cluster in the reduced form of [Fe]H₂ase places a CO underneath the Fe—Fe vector. Its bonding character depends on the enzyme redox level. IR spectral studies have found three different oxidation levels based on stretching frequencies of the diatomic ligands in [Fe]H₂ase (26). The results of H_{ox} and H_{red} corroborate the differences established in x-ray crystal structures, which found movement of the bridging CO in the H_{ox} to terminal in H_{red} (Fig. 2). Note that the mobile CO is trans to the cysteine sulfur that bridges to the proximal [4Fe4S] cluster. Thus as electrons enter or leave the dinuclear active-site cluster, the μ-CO is well situated to moderate charge differences with only minor structural changes. Interpretation of Mössbauer (44) and EPR data (45, 46) and correlation of IR spectra with model compounds (40) permit oxidation-state assignments of $Fe^{II}Fe^I$ to H_{ox} and Fe^IFe^I to H_{red}. The [4Fe4S] cluster maintains a $+2$ redox level in these two states, H_{ox} and H_{red} (44–46).

This bridging CO ($\approx 1,800$ cm^{-1}) in H_{ox}, which may exist as semibridging ($\approx 1,850$ cm^{-1}) or terminal (1,895 cm^{-1}) in the H_{red}, is one of the active-site features that small-molecule models have not yet been able to reproduce as ground-state, stable moieties. A second is the paramagnetic oxidized form of the enzyme, i.e., the $Fe^{II}Fe^I$ mixed-valent species. Such a lack of stability signals the important role of the protein in evolving or developing the active site to perform difficult functions with ease. Desirable properties as are elusive in thermodynamically stable model compounds, the structures of which are dictated solely by
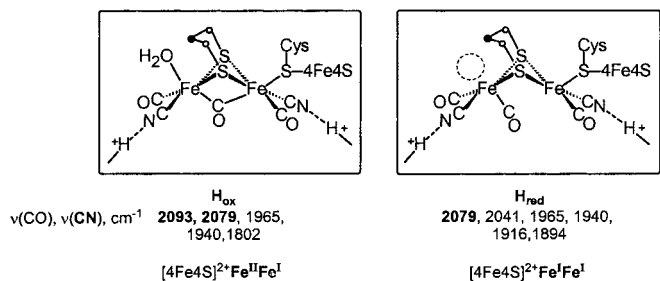

Fig. 2. Structures, ν(CO), ν(CN) stretching frequencies (26), and possible oxidation-state assignments of the oxidized (H_{ox}) and reduced (H_{red}) forms of the [Fe]H₂ase (44) (Fe···Fe distances are 2.6 Å for both).
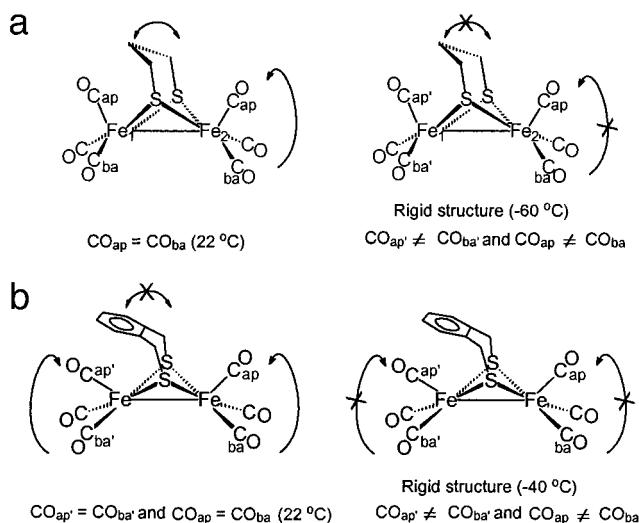
Darensbourg *et al.*

a

CO$_{ap}$ = CO$_{ba}$ (22 °C)

Rigid structure (-60 °C)
CO$_{ap'}$ ≠ CO$_{ba'}$ and CO$_{ap}$ ≠ CO$_{ba}$

b

CO$_{ap'}$ = CO$_{ba'}$ and CO$_{ap}$ = CO$_{ba}$ (22 °C)

Rigid structure (-40 °C)
CO$_{ap'}$ ≠ CO$_{ba'}$ and CO$_{ap}$ ≠ CO$_{ba}$

Fig. 3. Stereochemical nonrigidity of (μ-pdt)[Fe(CO)$_3$]$_2$ (*a*) and (μ-o-xyldt)[Fe(CO)$_3$]$_2$ (*b*).

HOMO

Mulliken charges:	Fe$_A$ -1.045	Fe$_A$ -0.998
	Fe$_B$ -1.031	Fe$_B$ -1.174
Fe···Fe (Å)	2.49	2.56

Fig. 4. Polarization of Fe—Fe bond electron density upon Fe(CO)$_3$ unit rotation in (μ-pdt)[Fe(CO)$_3$]$_2$ as shown by the highest occupied molecular orbitals (HOMOs) and the Mulliken charges.

first coordination sphere requirements of metal and ligand, require structural forms of higher energy, similar to intermediates or transition states along reaction paths or molecular rearrangement profiles. This is a statement of the entatic-state principle as expressed by Vallee and Williams in 1968 (47). The following summary of fundamental properties of {(μ-SRS)[Fe(CO)$_2$L]$_2$ (L = CO, CN$^-$, PMe$_3$)} model complexes provided the basis for this conclusion.

Stereochemical Nonrigidity of (μ-SRS)[Fe(CO)$_3$]$_2$ Model Complexes

An obvious structural feature of the (μ-SRS)[Fe(CO)$_3$]$_2$ complexes is the ease with which molecular rearrangements occur. Stereochemical nonrigidity exists in the iron dithiacyclohexane moiety of (μ-pdt)[Fe(CO)$_3$]$_2$ as shown by variable-temperature ^{1}H-NMR studies (48). In contrast, at 22°C the bridge is fixed in the (μ-o-xyldt)[Fe(CO)$_3$]$_2$, making the two iron atoms nonequivalent (Fig. 3).

Variable-temperature ^{13}C-NMR spectra established the intramolecular dynamics of the carbonyls in (μ-SRS)Fe$_2$(CO)$_6$ to be restricted to basal/apical CO site exchange in individual Fe(CO)$_3$ units (ref. 48; Fig. 3). This study found a lower rotational barrier for the (μ-o-xyldt)[Fe(CO)$_3$]$_2$ as compared with the other members of the series. Relief of the repulsive interaction of the arene group with the apical CO ligand, i.e., a steric assist to rotation, accounts for the lower barrier. This conclusion was corroborated and extended by density functional theory computations (49).

Fig. 4 presents results of density functional theory computations of the intramolecular CO-site exchange processes in (μ-pdt)[Fe(CO)$_3$]$_2$ (49). The computed activation barrier of 13.7 kcal/mol is consistent with that estimated from the NMR coalescence temperatures. More interesting is the change in the highest occupied molecular orbitals resulting from structural differences of ground-state and transition-state structures. The optimized transition-state geometry is not a simple 60° staggering of the eclipsed Fe(CO)$_3$ units in the ground-state structure. Rather, as the rotation occurs, the CO that comes underneath the Fe—Fe bond vector develops a slight bend concomitant with overall flattening of the rotated S$_2$Fe(CO)$_3$ unit.

If the ground-state (μ-pdt)[Fe(CO)$_3$]$_2$ is viewed as a symmetrical edge-bridged square pyramid, the transition state for Fe(CO)$_3$ rotation shows that one square pyramid is inverted relative to the other. Further consequences are: (*i*) there de-
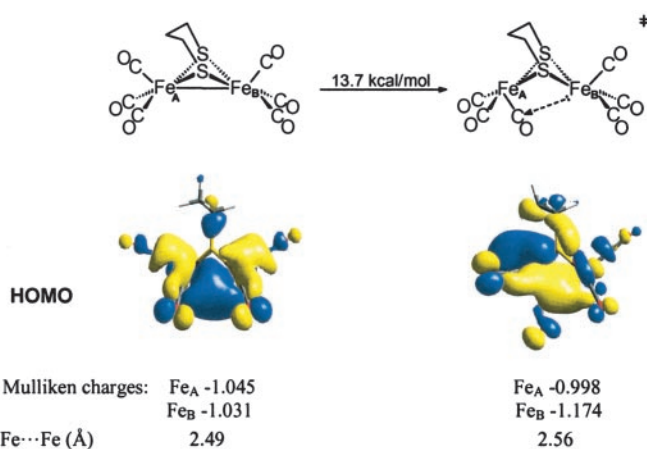
velops a partial disruption and lengthening of the Fe—Fe bond; (*ii*) the Fe—Fe bond density is polarized toward the unrotated iron; (*iii*) this polarized bond density is partially dispersed onto the CO group that lies underneath the Fe—Fe vector; and (*iv*) a charge disparity develops with the iron of the rotated Fe(CO)$_3$ unit being ≈0.2 units more positive and presenting itself with an apparent open site.

It did not go unnoticed that the transition-state structure of the model complex in such a rotated state, as shown in Fig. 4, resembled that of the reduced enzyme active site, perhaps implying that the latter has been trapped in a high-energy conformation, locked by H-bonding and other protein interactions in a position so as to readily perform functions of the catalyst. For example, if a better electron-donating ligand were to be trans to the incipient bridging CO group, a stronger donation from Fe$_B$ to the μ-CO should be possible, better "fixing" the structure. This position is occupied by the S of cysteine bridged to [4Fe4S] cluster in the enzyme active site. The steric interaction of the central unit in the irondithiacyclohexane ring is also expected to stabilize the rotated state. Such expectations gained credibility with further computations of isomeric forms of (μ-pdt)[Fe(CO)$_3$][Fe(CO)$_2$(CN)]$^-$ (49). Consistent with NMR results, the lowest barrier to rotation is for the Fe(CO)$_3$ unit within the monocyano derivative (Eq. **2**). The computations again found a steric assist to the rotation process.

[2]
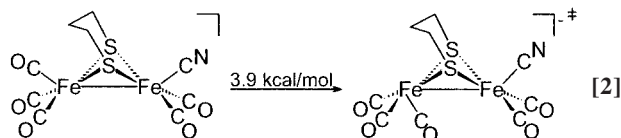
The dependence of configurational mobility on the steric nature of μ-SRS and the electronic character of the substituent ligand helped account for the R dependence in the cyanide substitution reactions, described below.

Chemical- and Regioselectivity in CN$^-$/CO Exchange Reactions in (μ-SRS)[Fe(CO)$_3$]$_2$: Reaction Profiles

Detailed kinetic studies (Eqs. **3** and **4**) established the CN$^-$/CO substitution process in (μ-SRS)[Fe(CO)$_3$]$_2$ [R = −CH$_2$CH$_2$− (edt), −CH$_2$CH$_2$CH$_2$− (pdt), or −CH$_2$C$_6$H$_4$CH$_2$− (o-xyldt)], which yields the disubstituted derivatives,

Fig. 6. Calculated and observed diiron complexes with a bridging CO group, closer structural analogues to the active site of [Fe]H$_2$ase.
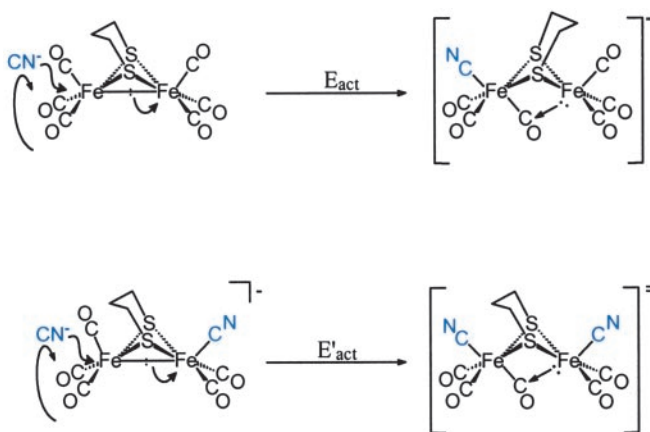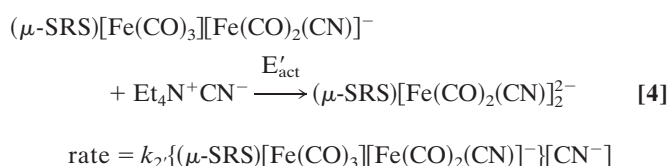
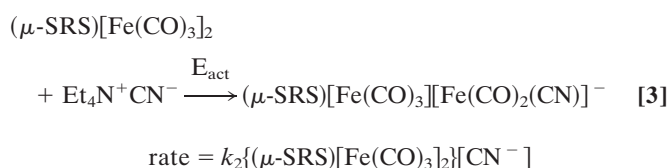Fig. 5. Proposed mechanism for the two-step CN$^-$/CO substitution reaction in (μ-pdt)[Fe(CO)$_3$]$_2$ to yield (μ-pdt)[Fe(CO)$_2$(CN)]$_2^{2-}$.

(μ-SRS)[Fe(CO)$_2$(CN)]$_2^{2-}$, is a two-step process in which both steps follow associative (S$_N$2) pathways (48).

(μ-SRS)[Fe(CO)$_3$]$_2$

$$+ \text{Et}_4\text{N}^+\text{CN}^- \xrightarrow{\text{E}_{\text{act}}} (\mu\text{-SRS})[\text{Fe(CO)}_3][\text{Fe(CO)}_2(\text{CN})]^- \quad \textbf{[3]}$$

$$\text{rate} = k_2\{(\mu\text{-SRS})[\text{Fe(CO)}_3]_2\}[\text{CN}^-]$$

(μ-SRS)[Fe(CO)$_3$][Fe(CO)$_2$(CN)]$^-$

$$+ \text{Et}_4\text{N}^+\text{CN}^- \xrightarrow{\text{E}'_{\text{act}}} (\mu\text{-SRS})[\text{Fe(CO)}_2(\text{CN})]_2^{2-} \quad \textbf{[4]}$$

$$\text{rate} = k_{2'}\{(\mu\text{-SRS})[\text{Fe(CO)}_3][\text{Fe(CO)}_2(\text{CN})]^-\}[\text{CN}^-]$$

The relative rates of addition of the cyanides has an R-dependent reactivity pattern that cannot be explained based on the electronic effect of the μ-SRS bridge; as indicated by the ν(CO) stretching frequencies of the (μ-SRS)[Fe(CO)$_3$]$_2$, all the bridges have similar electron donor abilities. For μ-SRS = μ-o-xyldt, E'_{act} is greater than E_{act}, whereas for μ-pdt, the opposite order was observed, $E_{\text{act}} > E'_{\text{act}}$! The latter result was unexpected, because nucleophilic attack of an anion on an anion typically results in rate inhibition. The origin of what appeared to be a co-operative effect of the first cyanide for addition of the second became a focus of study that involved the fundamental structural characteristics of dithiolatodiironhexacarbonyl complexes described above. The fact that the (μ-o-xyldt)[Fe(CO)$_3$]$_2$ that has a lower barrier of Fe(CO)$_3$ unit rotation demonstrated faster CN$^-$/CO reactivity suggests a connection between the mobility of the Fe(CO)$_3$ unit and the reactivity of the molecule toward CN$^-$. This relationship is embodied in the mechanism expressed in Fig. 5 as a possibility of CN$^-$/CO substitution reaction pathway. It resolves the overall activation energy, E_{act}(overall), into two processes: CN$^-$ attack, E_{act}(CN$^-$ attack); and rotation, E_{act}(rot'n) (Eq. **5**).

$$E_{\text{act}}(\text{overall}) = E_{\text{act}}(\text{CN}^- \text{ attack}) + E_{\text{act}}(\text{rot'n}) \quad \textbf{[5]}$$

Thus the proposed mechanism for the CN$^-$ displacement of CO given in Fig. 5 provides rationale for the cooperative effect of the intrinsic cyanide during the nucleophilic attack of the second CN$^-$. The S$_N$2 character of the cyanide reaction results in displacement of the Fe—Fe bond density concomitant with rotation of the Fe(CO)$_3$ unit, positioning one CO underneath the Fe—Fe vector and aiding in delocalizing the electron density
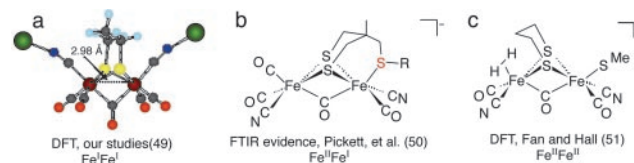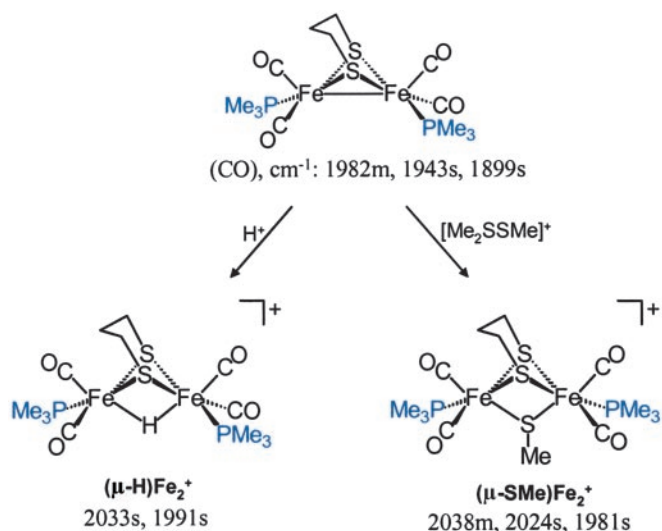
that was displaced toward the unrotated iron. According to this mechanism the second CN$^-$ finds a lower rotational barrier due to the presence of the already coordinated anionic CN$^-$ ligand, which stabilizes the resulting bridging CO and the rotated form of the inverted square pyramid. This explains the similarity of the activation parameters for the second CN$^-$ addition for both the aliphatic (pdt and edt) and aromatic (o-xyldt) bridges. In the case of the (μ-o-xyldt)[Fe(CO)$_3$]$_2$ there is an assist even for the first CN$^-$ attack. It comes from the repulsive CO/arene interaction that lowers the rotational barrier and, as a result, the activation energy for the first CN$^-$ addition. Because this assist is missing from the edt completely and is less substantial for the pdt bridge, the first CN$^-$ attack finds a higher activation barrier in these binuclear complexes of aliphatic bridges as compared with the aromatic o-xyldt.

Such a hypothesis as presented for the CN$^-$/CO substitution mechanism has been supported by density functional theory calculations of the Fe(CO)$_3$ unit rotation in (μ-pdt-)[Fe(CO)$_3$]$_2$, which compared the various transition-state possibilities of (μ-pdt)[Fe(CO)$_3$]$_2$ and (μ-pdt)[Fe(CO)$_3$][Fe(CO)$_2$CN]$^-$ as discussed earlier. That the second CN$^-$ attack process might have a similar barrier to the first bespeaks the increased stabilization of the rotated Fe(CO)$_3$ unit when the adjacent iron atom is rendered more electron-rich in the Fe(CO)$_2$(CN) form.

The extent of the actual bridging character of that CO group positioned beneath the Fe—Fe vector increases as the entering CN$^-$ docks into the opened coordination position on iron. This conclusion is based on density functional theory computations of the reaction profile of the CN$^-$/CO substitution process, which includes the intermediate shown in Fig. 6a (49). In this study a sodium cyanide ion pair in the form of CN$^-$···Na$^+$ was used instead of CN$^-$ to avoid the charge difference between the species involved in the process. More definite evidence for such a μ-CO as might be in the CO-inhibited, oxidized form of the enzyme comes from Fourier transform IR spectral data of an electrochemically generated Fe^{II}Fe^I, Fe$_2$S$_3$ complex, which shows an almost precise match of the ν(CN), ν(CO) values with those of the enzyme (Fig. 6b; ref. 50). The η^2–H$_2$ complex indicated in Fig. 6c results from the theoretical modeling of the functioning enzyme active site (51); its binding or stabilization requires d^6 Fe^{II}.

The Quest for Models that Function as Does the [Fe]H$_2$ase Active Site

H$_2$ Uptake. The structural match of the rotated, transition-state form of (μ-SRS)[Fe(CO)$_3$]$_2$ model complexes with the enzyme active site does not provide a functional similarity. The all-carbonyl complex does not take up a proton, nor does it bind molecular H$_2$. In a reduced Fe^{I}Fe^I form the enzyme active site performs the former, whereas the latter requires the one-electron more-oxidized form, Fe^{II}Fe^I. Although Pickett and coworkers (50) have reported evidence for such a species from spectroelectrochemical studies, such a stable mixed-valent species is not achieved easily in the chemist's laboratory. However, the binuclear Fe^{I}Fe^I complexes, rendered more electron-rich by CO exchange with PMe$_3$, react with electrophiles,

(CO), cm^{-1}: 1982m, 1943s, 1899s

H$^+$ [Me$_2$SSMe]$^+$

(μ-H)Fe$_2$$^+$
2033s, 1991s

(μ-SMe)Fe$_2$$^+$
2038m, 2024s, 1981s

Scheme 1. Binuclear oxidative addition of electrophiles H$^+$ and SMe$^+$ to Fe^{I}Fe^I.

E$^+$, and engage the Fe^{I}Fe^I-bond density in binuclear oxidative addition, yielding Fe^{II}Fe^{II} species in the form of (μ-E)(μ-pdt)[Fe(CO)$_2$(PMe$_3$)]$_2^+$ (Scheme 1; refs. 52–54).

Both d^6 Fe(II) binuclear complexes in Scheme 1 were shown to (*i*) have photochemically labile CO groups and (*ii*) mediate isotopic scrambling in H$_2$/D$_2$O or D$_2$/H$_2$O mixtures under photolytic conditions (52–54). Such H/D-exchange reactions are consistent with H$_2$ase activity test reactions. A possible mechanism for this exchange is given in Scheme 2 in which the open site for H$_2$ binding is positioned trans to the bridging ligand (H or SMe) similarly to the enzyme active site in which the H$_2$ binds trans to the bridging CO group. In the presence of water, mixtures of H$_2$ and D$_2$ also show isotopic scrambling to HD, with both E = H or SMe. In the absence of water, only the (μ-H)(μ-pdt)[Fe(CO)$_2$(PMe$_3$)]$_2^+$ has the capability to catalyze H/D exchange in mixtures of H$_2$ and D$_2$ to produce HD (52, 53).

It must be stressed that the Fe^{II}Fe^{II}-bridging hydride complexes serve to provide a functional model, the similarity to the enzyme active site of which rests in their binuclearity, their Fe$_2$S$_2$ core, and their ability to bind and heterolytically activate H$_2$ or D$_2$ at an Fe^{II} site. We do not wish to imply that a (μ-H)(μ-SRS)Fe$_2^+$ core exists in the enzyme active site. Rather the (μ-SRS)Fe^{II}Fe^I core is created electrochemically from (μ-SRS)(Fe^I)$_2$, generating a coordinately unsaturated,
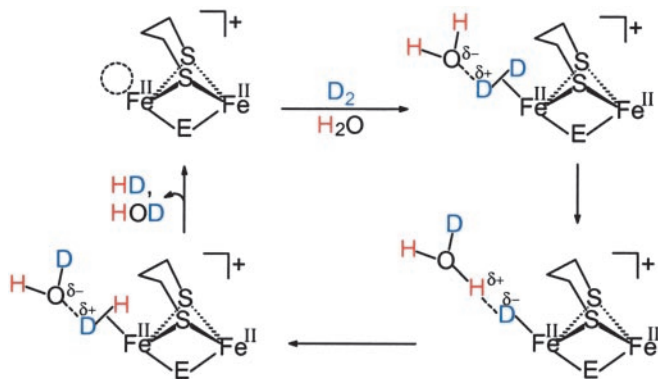

Scheme 2. H/D exchange mechanism.

ECCE
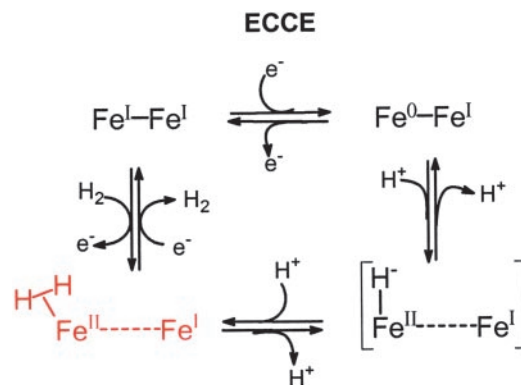
Scheme 3. Mechanism for electrocatalytic production of H$_2$.

16-e$^-$, Fe^{II} center, the ground-state structure of which matches the expected transition state in our ligand substitution reactions in (μ-SRS)[Fe(CO)$_3$]$_2$. It also matches the transition state and intermediate in the coordinately unsaturated (μ-E)(μ-SRS)Fe$^{II}_2$ that serves to bind and activate H$_2$.

H$_2$ Production Mechanisms. The expected prominent intermediate in H$_2$ uptake by the [Fe]H$_2$ase active site shown below is, by microscopic reversibility, present in H$_2$ production. Rates of proton and electron transfer to the site as well as H$_2$ release account for the rapid rates of H$_2$ production in [Fe]H$_2$ases.
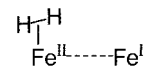
Thus the (η^2–H$_2$)Fe^{II}–Fe^I species is a principal in several electrochemical paths, deriving from iron(I) complexes as inaugural points. The electrochemical-chemical-chemical-electrochemical process expressed (clockwise from Fe^I–Fe^I) in Scheme 3 (D. Chong, I.P.G., M. L. Miller, R. Mejia-Rodriguez, and M.Y.D., unpublished data) has reduction to the Fe^{0}Fe^I mixed-valent species preceding protonation. This mechanism applies to the neutral Fe^I–Fe^I model complexes, (μ-SRS)[Fe(CO)$_2$L]$_2$ (L = CO or PMe$_3$), in the presence of acetic acid in CH$_3$CN solvent. Electrochemical studies in our laboratories (D. Chong, I.P.G., M. L. Miller, R. Mejia-Rodriguez, and M.Y.D., unpublished data) and others (55) verify catalytic H$_2$ production at potentials that depend on the donor ability of L and to a lessor extent on the nature of R. The all-CO complex better stabilizes the reduced Fe^{0}Fe^I intermediate, and produces H$_2$ at potentials ≈500 mV more positive than the complex with L = PMe$_3$. The latter complex, however, enjoys greater stability over long periods of electrolysis. It is also expected (as yet not demonstrated) to be more apt to participate in the reverse, H$_2$ uptake electrocatalytic process as the PMe$_3$ ligand better stabilizes Fe^{II}. The mixture of carbon monoxide and cyanide ligands (with H bonding to the cyanide-nitrogen) permits such catalytic tuning and control in the enzyme active site.

Conclusions

The fundamental characteristics that lead to H$_2$ase-like reactivity in the binuclear complexes that serve as structural models of [Fe]H$_2$ase provide a firm reference point for the oxidation states that are needed for H$^+$ or H$_2$ uptake and correlate redox levels with directionality of H$_2$ reactivity. The extremely fast turnovers of H$_2$ production in the [Fe]H$_2$ase (estimated at 9,000 molecules of H$_2$ per sec at 30°C for *Desulfovibrio desulfuricans*) (56) suggest that major structural rearrangements

are not occurring during the catalytic process. Thus the structural integrity of the "rotated" state, or inverted square pyramid shown below as the H_2 production form of the active site, permits electron density to flow from the [4Fe4S] "wire" into the Fe—Fe bond. Polarization onto the distal iron results in monocentric oxidative addition of a proton to Fe^0 and generates Fe^{II}–H and, after addition of the second proton, the η^2–H_2. Although release of H_2 is rapid in an electron-rich environment, the site accommodates binding H_2 as a nucleophile, when electron flow is reversed into the [4Fe4S] cluster. The CO that was terminal and permitted Fe⋯Fe contact in the H_2-producing mode now becomes bridging to better stabilize electron-deficient structures.
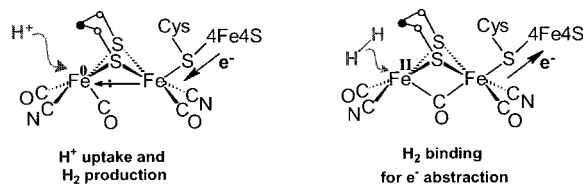
The reversibility of the reaction performed by the H_2ase enzyme may rest in the minimal active-site conformational changes. Protonation of the Fe^IFe^I model complexes in their ground states yields stable bridging hydrides that are not susceptible to subsequent protonation without the input of electrons at electropotentials much more negative that those observed in the enzyme. The formation of the bridging hydrides is prevented in a similarly reduced form of the active site of the enzyme by virtue of the rotated structure that positions a CO group beneath the Fe—Fe bond vector.

Of the many binuclear active sites now known to exist in metalloenzymes, that of the [Fe]H_2ase is arguably the simplest. It is attached to the protein by only one covalently bound ligand and a few H bonds. The points of catalytic control are subtle and apparently involve low energy and minor molecular motions within the first coordination sphere once it is poised in an orientation conducive to its chemical performance.

1. Stephenson, M. & Stickland, L. H. (1931) *Biochem. J.* **25,** 205–214.
2. Adams, M. W. W., Mortenson, L. E. & Chen, J.-S. (1981) *Biochim. Biophys. Acta* **594,** 105–176.
3. Graf, E.-G. & Thauer, R. K. (1981) *FEBS Lett.* **136,** 165–169.
4. Cammack, R., Frey, M. & Robson, R., eds. (2001) *Hydrogen as a Fuel* (Taylor & Francis, London).
5. Hoffmann, P. (2001) *Tomorrow's Energy: Fuel Cells, and Prospects for a Cleaner Planet* (MIT Press, Cambridge, MA).
6. Farkas, A., Farkas, L. & Yudkin, J. (1934) *Proc. R. Soc. London Ser. B* **115,** 373–379.
7. Krasna, A. I. & Rittenberg, D. (1954) *J. Am. Chem. Soc.* **76,** 3015–3020.
8. Ungváry, F. (1972) *J. Organomet. Chem.* **36,** 363–370.
9. Lespinat, P. A., Berlier, Y., Fauque, G., Czechowski, M., Dimom, B. & LeGall, J. (1986) *Biochimie* **68,** 55–61.
10. Teixeira, M., Fauque, G., Moura, I., Lespinat, P. A., Berlier, Y., Prickril, B., Peck, H. D., Jr., Xavier, A. V., LeGall, J. & Moura, J. J. G. (1987) *Eur. J. Biochem.* **167,** 47–58.
11. Albracht, S. P. J. (1994) *Biochim. Biophys. Acta* **1188,** 167–204.
12. Vignais, P. M., Billoud, B. & Meyer, J. (2001) *FEMS Microbiol. Rev.* **25,** 455–501.
13. Frey, M. (2002) *Chembiochem* **3,** 153–160.
14. Halpern, J. & Milne, J. B. (1960) *Proc. Int. Congr. Catal., 2nd* **1,** 445–457.
15. Halpern, J. (1980) *J. Organomet. Chem.* **200,** 133–144.
16. Kubas, G. J., Ryan, R. R., Swanson, B. I., Vergamini, P. J. & Wasserman, H. J. (1984) *J. Am. Chem. Soc.* **106,** 451–452.
17. Kubas, G. J. (1988) *Acc. Chem. Res.* **21,** 120–128.
18. Wächtershäuser, G. (1992) *Prog. Biophys. Mol. Biol.* **58,** 85–201.
19. Adams, M. W. W. & Stiefel, E. I. (2000) *Curr. Opin. Chem. Biol.* **4,** 214–220.
20. Garcin, E., Vernède, X., Hatchikian, E. C., Volbeda, A., Frey, M. & Fontecilla-Camps, J. C. (1999) *Structure (London)* **7,** 557–566.
21. Volbeda, A., Garcin, E., Piras, C., De Lacey, A. L., Fernandez, V. M., Hatchikian, E. C., Frey, M. & Fontecilla-Camps, J. C. (1996) *J. Am. Chem. Soc.* **118,** 12989–12996.
22. Bagley, K. A., Van Garderen, C. J., Chen, M., Duin, E. C., Albracht, S. P. J. & Woodruff, W. H. (1994) *Biochemistry* **33,** 9229–9236.
23. Pierik, A. J., Roseboom, W., Happe, R. P., Bagley, K. A. & Albracht, S. P. J. (1999) *J. Biol. Chem.* **274,** 3331–3337.
24. Peters, J. W., Lanzilotta, W. N., Lemon, B. J. & Seefeldt, L. C. (1998) *Science* **282,** 1853–1858.
25. Nicolet, Y., Piras, C., Legrand, P., Hatchikian, C. E. & Fontecilla-Camps, J. C. (1999) *Structure (London)* **7,** 13–23.
26. Nicolet, Y., De Lacey, A. L., Vernède, X., Fernandez, V. M., Hatchikian, E. C. & Fontecilla-Camps, J. C. (2001) *J. Am. Chem. Soc.* **123,** 1596–1601.
27. Lemon, B. J. & Peters, J. W. (1999) *Biochemistry* **38,** 12969–12973.
28. Van der Spek, T. M., Arendsen, A. F., Happe, R. P., Yun, S., Bagley, K. A., Stufkens, D. J., Hagen, W. R. & Albracht, S. P. J. (1996) *Eur. J. Biochem.* **237,** 629–634.
29. Pierik, A. J., Hulstein, M., Hagen, W. R. & Albracht, S. P. J. (1998) *Eur. J. Biochem.* **258,** 572–578.
30. Cody, G. D., Boctor, N. Z., Filley, T. R., Hazen, R. M., Scott, J. H., Sharma, A. & Yoger, H. S., Jr. (2000) *Science* **289,** 1337–1340.
31. Reihlen, H., Gruhl, A. & Hessling, G. (1929) *Liebigs Ann. Chem.* **472,** 268–287.
32. Hieber, W. & Spacu, P. (1937) *Z. Anorg. Allg. Chem.* **233,** 852–864.
33. Seyferth, D., Henderson, R. S. & Song, L.-C. (1982) *Organometallics* **1,** 125–133.
34. Seyferth, D., Womack, G. B., Gallagher, M. K., Cowie, M., Hames, B. W., Fackler J. P., Jr., & Mazany, A. M. (1987) *Organometallics* **6,** 283–294.
35. Winter, A., Zsolnai, L. & Huttner, G. (1982) *Z. Naturforsch., B: Anorg. Chem., Org. Chem.* **37,** 1430–1436.
36. Lyon, E. J., Georgakaki, I. P., Reibenspies, J. H. & Darensbourg, M. Y. (1999) *Angew. Chem. Int. Ed. Engl.* **38,** 3178–3180.
37. Schmidt, M., Contakes, S. M. & Rauchfuss, T. B. (1999) *J. Am. Chem. Soc.* **121,** 9736–9737.
38. Le Cloirec, A., Best, S. P., Borg, S., Davies, S. C., Evans, D. J., Hughes, D. L. & Pickett, C. J. (1999) *Chem. Commun.*, 2285–2286.
39. Nicolet, Y., Lemon, B. J., Fontecilla-Camps, J. C. & Peters, J. W. (2000) *Trends Biochem. Sci.* **25,** 138–143.
40. De Lacey, A. L., Stadler, C., Cavazza, C., Hatchikian, E. C. & Fernandez, V. M. (2000) *J. Am. Chem. Soc.* **122,** 11232–11233.
41. Chen, Z., Lemon, B. J., Huang, S., Swartz, D. J., Peters, J. W. & Bagley, K. A. (2002) *Biochemistry* **41,** 2036–2043.
42. Fan, H.-J. & Hall, M. B. (2001) *J. Am. Chem. Soc.* **123,** 3828–3829.
43. Li, H. & Rauchfuss, T. B. (2002) *J. Am. Chem. Soc.* **124,** 726–727.
44. Popescu, C. V. & Münck, E. (1999) *J. Am. Chem. Soc.* **121,** 7877–7884.
45. Pereira, A. S., Tavares, P., Moura, I., Moura, J. J. G. & Huynh, B. H. (2001) *J. Am. Chem. Soc.* **123,** 2771–2782.
46. Bennett, B., Lemon, B. J. & Peters, J. W. (2000) *Biochemistry* **39,** 7455–7460.
47. Vallee, B. L. & Williams, R. J. (1968) *Proc. Natl. Acad. Sci. USA* **59,** 498–505.
48. Lyon, E. J., Georgakaki, I. P., Reibenspies, J. H. & Darensbourg, M. Y. (2001) *J. Am. Chem. Soc.* **123,** 3268–3278.
49. Georgakaki, I. P., Thomson, L. M., Lyon, E. J., Hall, M. B. & Darensbourg, M. Y. (2003) *Coord. Chem. Rev.*, in press.
50. Razavet, M., Borg, S. J., George, S. J., Best, S. P., Fairhurst, S. A. & Pickett, C. J. (2002) *Chem. Commun.*, 700–701.
51. Cao, Z. X. & Hall, M. B. (2001) *J. Am. Chem. Soc.* **123,** 3734–3742.
52. Zhao, X., Georgakaki, I. P., Miller, M. L., Yarbrough, J. C. & Darensbourg, M. Y. (2001) *J. Am. Chem. Soc.* **123,** 9710–9711.
53. Zhao, X., Georgakaki, I. P., Miller, M. L., Mejia-Rodriguez, R., Chiang, C.-Y. & Darensbourg, M. Y. (2002) *Inorg. Chem.* **41,** 3917–3928.
54. Georgakaki, I. P., Miller, M. L. & Darensbourg, M. Y. (2003) *Inorg. Chem.*, in press.
55. Gloaguen, F., Lawrence, J. D. & Rauchfuss, T. B. (2001) *J. Am. Chem. Soc.* **123,** 9476–9477.
56. Cammack, R. (1999) *Nature* **397,** 214–215.